

# Eco-friendly Synthesis of Silver Nanoparticles and its Application in Hydrogen Photogeneration and Nanoplasmonic Biosensing

Guilherme B. Strapasson<sup>+</sup>,<sup>[a]</sup> Eduarda de C. Flach<sup>+</sup>,<sup>[a]</sup> Marcelo Assis,<sup>[b]</sup> Silma A. Corrêa,<sup>[a]</sup> Elson Longo,<sup>[c]</sup> Giovanna Machado,<sup>[d]</sup> Jacqueline F. L. Santos,<sup>[a]</sup> and Daniel E. Weibel<sup>\*[a]</sup>

Environmentally friendly methods for silver nanoparticles (AgNPs) synthesis without the use of hazardous chemicals have recently drawn attention. In this work, AgNPs have been synthesized by microwave irradiation using only honey solutions or aqueous fresh pink radish extracts. The concentrations of honey, radish extract, AgNO<sub>3</sub> and pH were varied. AgNPs presented mean sizes between 7.0 and 12.8 nm and were stable up to 120 days. The AgNPs were employed as co-catalyst (TiO<sub>2</sub>@AgNPs) to increase the hydrogen photogeneration under

UV-vis and only visible light irradiation, when compared to pristine TiO<sub>2</sub> NPs. The prepared photocatalyst also showed hydrogen generation under visible light. Additionally, AgNPs were used to assemble a nanoplasmonic biosensor for the biodetection of extremely low concentrations of streptavidin, owing to its specific binding to biotin. It is shown here that green AgNPs are versatile nanomaterials, thus being potential candidates for hydrogen photogeneration and biosensing applications.

## Introduction

Noble metal nanoparticles (NMNPs) are extensively used in various applications, such as sensors, catalysis, photocatalysis, and medicine, due to their exceptional optical, thermal, and electrical properties. In particular, silver nanoparticles (AgNPs) have become one of the most employed and versatile materials among NMNPs because of their unique physical and chemical properties. As a consequence, there is an important demand to develop environment-friendly techniques with non-toxic chemicals for AgNP synthesis. The increasing demand for green synthesis and production of NPs was evidenced by the merging of new cost-effective and eco-friendly techniques. These

methodologies are trying to integrate green chemistry principles and NPs production for specific applications, such as in the textile industry due to the well known antimicrobial activity of the AgNPs.

Many distinct types of extracts and synthetic methods can be found for AgNPs preparation.<sup>[1]</sup> For example, AgNPs of about 65 nm in size were prepared using corn starch as stabilizer and reducing agent and sodium citrate as an additional reducing agent.<sup>[2]</sup> Finally, the NPs were loaded with Isoorientin (Iso), a natural flavonoid, showing high stability in the simulated gastrointestinal digestion and low in vitro cytotoxicity. Other nanostructured materials were also prepared using different aqueous extracts, such as *Rosa santana* petals,<sup>[3]</sup> *Moringa oleifera* seed,<sup>[4]</sup> *Chara Algae*<sup>[5]</sup> and several more.<sup>[6,7]</sup> Biological synthesis is also a methodology employed for the NMNPs,<sup>[8]</sup> but it is often time-consuming and require sterilized conditions. On the other hand, green synthesis methodologies can overcome those drawbacks.

The variable chemical composition and antioxidant properties of some foods have also been under investigation for the syntheses of NMNPs. Natural honey, probably one of the oldest sweet food sources, is an excellent medium for NMNPs preparation. Honey is rich in carbohydrates (80–85%) containing mainly glucose and fructose, water (15–17%), proteins, amino acids, enzymes, antioxidants, vitamins, and important minerals (K and Mg).<sup>[9]</sup> The natural honey composition depends on the plant and bee species, climate, and vegetation. Probably the first syntheses of NMNPs using honey as reducing and capping agent was reported more than a decade ago.<sup>[10]</sup> That work, carried out at room temperature, showed the viability of the biosynthesis of gold nanoparticles (AuNPs) together with an increase in productivity compared to other biosynthesis routes already reported at that time.


[a] G. B. Strapasson,<sup>+</sup> E. de C. Flach,<sup>+</sup> Prof. S. A. Corrêa, Prof. J. F. L. Santos, Prof. D. E. Weibel  
Institute of Chemistry, Universidade Federal do Rio Grande do Sul, UFRGS, Av. Bento Gonçalves 9500, P.O.Box 15003, 91501-970, Porto Alegre, RS, Brazil  
E-mail: danielw@iq.ufrgs.br  
Homepage: <https://pnipe.mctic.gov.br/search?term=lafos&type=LAB>

[b] Dr. M. Assis  
Department of Analytical and Physical Chemistry, University Jaume I (UJI), Castelló, 12071, Spain

[c] Prof. E. Longo  
CDMF, Federal University of Sao Carlos - UFSCar, P.O. Box 676, 13565e905, São Carlos, São Paulo, Brazil

[d] Dr. G. Machado  
Centro de Tecnologias Estratégicas do Nordeste (CETENE)  
Av. Prof. Luis Freire, n° 01 – Cidade Universitária – Recife/PE, Brazil, CEP: 50.740-545  
and  
GBS: Current Address: Institute of Chemistry, University of Campinas, UNICAMP, Campinas, 13083-970, São Paulo, Brazil

[<sup>+</sup>] These authors contributed equally to this work

 Supporting information for this article is available on the WWW under <https://doi.org/10.1002/cphc.202300002>

Several reports have been published in the following years using honey as the main green medium for NMNPs preparation. For example, AuNPs were obtained by hydrolytic polycondensation of tetraethoxysilane in aqueous solutions of honey containing  $\text{HAuCl}_4$  and HCl as acid catalyst.<sup>[11]</sup> Spherical particles of about 7 nm in diameter were formed in the regions of the organosilicon sol, but outside the sol the NPs size increased up to 40–50 nm. Kumar et al. demonstrated that AgNPs can also be obtained from a sunlight-induced green synthesis methodology.<sup>[12]</sup> By using 3% honey aqueous solution and  $0.1 \text{ mol L}^{-1}$   $\text{AgNO}_3$ , it was possible to prepare AgNPs between 2–4 nm and 20–30 nm in size. The NPs presented, according to the authors, excellent antimicrobial activity against *E. coli*, *Klebsiella* and *S. aureus*. Spherical copper NPs (CuNPs) of 3.68 nm in size were prepared by ultrasonic irradiation with a 10% w/v concentration of honey added into the copper nitrate solution containing ascorbic acid ( $1 \text{ mol L}^{-1}$ ).<sup>[13]</sup> The CuNPs presented antibacterial activity against gram-positive and gram-negative bacteria (*Enterococcus faecalis* and *Escherichia coli* respectively). Nickel NPs between 28–31 nm in diameter were prepared using honey as bio-supported reducing agent.<sup>[14]</sup> The study involved changes in pH, temperature, concentration of honey as reducing agent and the results were compared with a predictive mathematical methodology.

Another eco-friendly method for obtaining AgNPs is by using radish, which is a root vegetable from the *Cruciferaeae* family. Radish has high antioxidant properties that are attributed to its main phenolic components, sinapic acid esters, and flavonoids, making it an interesting food to explore.<sup>[15]</sup> Radish is an important vegetable crop worldwide and its properties have already been reported to some extent.<sup>[16–18]</sup> In South America radish has received recently some interest concerning its phytochemical composition where 8 radish varieties and their antioxidant properties were investigated.<sup>[19]</sup> The physicochemical properties of red radish and its antioxidant capacity of fresh leaves and roots were also objects of study.<sup>[20]</sup>

AgNPs stand out due to their potential to be applied in different fields and their excellent properties. For instance, their optical property, in addition to the redox capacity and surface area, improve their performance as catalysts, co-catalysts, or photocatalysts. Their well-known optical behavior is associated with the localized surface plasmon resonance (LSPR) that arises from the collective oscillation of the metallic particle's electrons with the incident electromagnetic radiation.<sup>[21]</sup> This phenomenon is very sensitive to the environment, for example, when the refractive index near the NMNPs surface changes by the adsorption of molecules.<sup>[22]</sup> The resulting larger charge separation and a weaker restoring force lead to a red shift in the plasmonic band, which is the base for their application in nanoplasmonic biosensing.<sup>[23]</sup> Green synthesized NMNPs have been used as nanoplasmonic sensor in phase configuration for different analytes, for instance, AgNPs have been employed in the determination of copper, mercury, zinc, and lead.<sup>[24,25]</sup>

AgNPs have many potential biomedical applications due to their low cytotoxicity and effective antibacterial and antimicrobial activities. Typical applications of green AgNPs synthesis usually involve testing those actions.<sup>[26]</sup> Studying green AgNPs

in other important fields, such as photocatalysis, hydrogen photogeneration, or sensors, is also highly relevant. A few works have been reported in the fields of preparation of biosensors<sup>[27,28]</sup> or photocatalysis for degradation of dyes using green AgNPs as co-catalysts.<sup>[27,29–31]</sup> Despite a green method for the fabrication of NMNPs being vital, to the best of our knowledge, there are almost no studies using only aqueous radish extract as both reducing and stabilizing species for the synthesis of AgNPs. While in the case of natural honey there are only a few reports on its use for the fabrication of AgNPs using microwave-assisted (MW) methodologies.

The AgNPs prepared using honey were impregnated onto  $\text{TiO}_2$  NPs and were employed as co-catalyst for the photogeneration of hydrogen in the photo-reform of methanol. Hydrogen evolved steadily under UV-Vis and only visible light irradiation at room temperature. The AgNPs synthesized with radish extract were used for the assemble a nanoplasmonic biosensor chip to evaluate the potential of detecting biomarkers using the interaction between biotin and streptavidin as a model system. The AgNPs were also prepared using extracts from the skin and even from rotten radish. UV-vis spectroscopy, transmission electron microscopy (TEM), X-ray photoelectron spectroscopy (XPS), and Fourier transform infrared spectroscopy (FTIR) were used for the AgNPs characterization.

## Results and Discussion

### Green AgNPs characterization

Eco-friendly syntheses of AgNPs were conducted using honey solutions or radish extract and the following synthesis parameters were varied: honey solution and extract concentrations,  $\text{AgNO}_3$  concentration, and pH. The change in the color of the reaction mixture after 30 seconds of microwave irradiation from yellow-yellowish brown to deep brown was a clear indication of the AgNPs formation. The images of the as synthesized AgNPs for honey and radish extract evidenced their efficient formation (see Figures S1–S3 and Figures S4–S5, respectively). The formation of AgNPs was further confirmed by its SPR effect,<sup>[32]</sup> which results in the characteristic absorption band in the 400–500 nm region. The wavelength at the maximum absorption ( $\lambda_{\text{max}}$ ) and the Full Width at Half Maximum (FWHM) of the SPR band can be associated with the mean size and size distribution of the NPs, respectively. Therefore, the UV-Vis spectra data provides important insights into the effect of synthesis parameters.

Sharp and intense SPR bands centered at  $\sim 410$  nm (Figure 1a) were obtained when the honey concentration was  $0.6 \text{ g mL}^{-1}$  or higher. Moreover, there was almost no change in the  $\lambda_{\text{max}}$  and FWHM when the concentration of honey further increased (see Table S1). These results could be associated with the presence of a dense medium at higher honey concentrations, containing sufficiently reducing and stabilizing agents, which avoided AgNPs aggregation or etching.<sup>[32]</sup> At lower honey solution concentrations the NPs are not sufficiently covered with the stabilizing molecules leading to the coalescence and

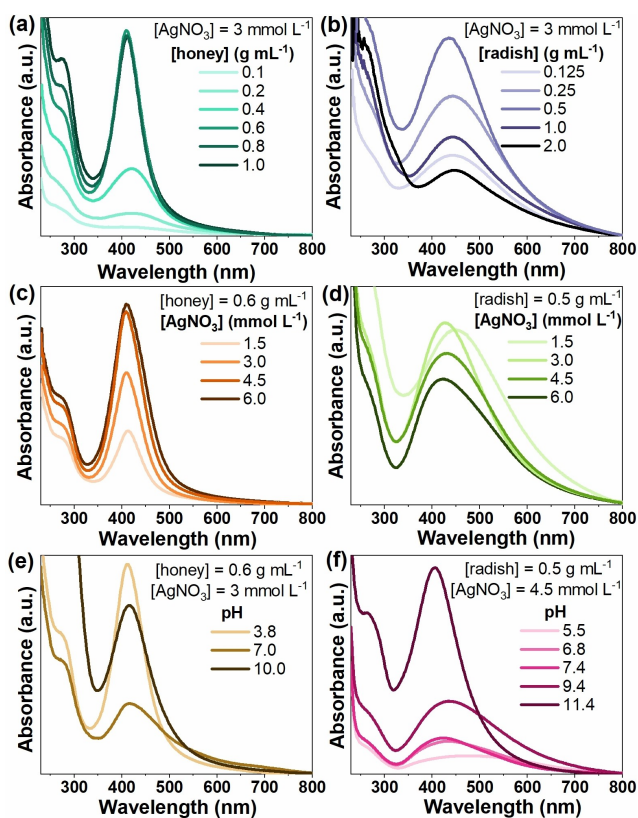


**Figure 1.** UV-Vis spectra of AgNPs prepared under various synthesis parameters using: aqueous honey solutions (a), (c) and (e); and aqueous radish extract solutions (b), (d) and (f). Microwave irradiating time: 30 seconds

heterogeneous distribution of sizes, as suggested by their larger FWHM (Table S1). Slight pH variations of the honey solutions were also observed, becoming more acidic as the honey concentration increased (Table S2). Figure 1c shows that when the concentration of honey is constant ( $0.6 \text{ mmol L}^{-1}$ ), the intensity of the SPR band increased alongside the increase in the  $\text{AgNO}_3$  concentration. Almost no change was observed on the  $\lambda_{\text{max}}$  and FWHM (Table S1), demonstrating that the obtained NPs have similar mean sizes and size distributions even with different  $\text{AgNO}_3$  concentrations.

The dependence of the AgNPs optical properties on the synthesis pH was studied in some detail (see also Table S1 and Figure S3). The UV-Vis spectra show sharp and intense absorption bands centered at 410–414 nm with FWHM of 78 nm and 82 nm for the acidic and alkaline mediums, respectively. In the synthesis of Ag and AuNPs by electron irradiation, the authors inferred that the mechanism of formation of the NPs was originated by the formation of electrons and hydrogen atoms that can act as reducing agents for converting metal ions to lower valence atoms or even neutral ones.<sup>[33]</sup> The proton-rich medium may contribute to improving the nucleation step during the formation of the AgNPs, once they function as additional reducing reactants in the medium. The high irradiation conditions of microwave excitation may lead to similar results. Differently, the hydroxyl groups can improve the reaction rate by oxidizing the silver atoms forming  $\text{Ag}_2\text{O}$  or

$\text{Ag}(\text{OH})_x$  species with increasing NaOH concentration, as previously evidenced by XAFS and XANES analysis.<sup>[34]</sup> Again, the formation of reactive species from the extract might be induced with microwave irradiation (Figure S6). At pH 7.0 there was a dampening in the absorbance, presenting a broader SPR band (FWHM = 102 nm). This behavior is an indicator of a coalescent growth mechanism, where smaller particles aggregate to produce larger particles, resulting in the reduction of the total number of particles within the solution.

Radish extract was also used for the AgNPs preparation and the dependence of the nanoparticle growth on the chemical composition of the extract was investigated. The effect of radish extract and  $\text{AgNO}_3$  concentrations (Figure 1b and Figure 1d) demonstrated an optimum synthesis condition, blue-shifted plasmon band, and lower FWHM using  $3 \text{ mmol L}^{-1}$  of  $\text{AgNO}_3$  and  $0.5 \text{ g mL}^{-1}$  radish extract (see Table S3). The method for synthesizing AgNPs was applied to both fresh and rotten radishes, including their skins (see Figure S7). This shows that food scraps such as the radish skin or rotten radish can be reused for the AgNPs preparation.

When the radish extract and  $\text{AgNO}_3$  concentrations were higher, a well-noticed dampening in the intensity was observed. In Figure 1b, one can also notice an apparent red shift in the SPR bands (Table S3). These results may indicate a smaller number of nanoparticles in suspension, larger diameter and size distribution, characteristics of the coalescence. Previous works have shown typical bell-shaped curves of dose-response data for SPR maximum as a function of the extract concentration.<sup>[8,35]</sup> For example, in the biosyntheses of AgNPs using *Artemisia absinthium* aqueous extract, the authors hypothesized that the obtained results indicated that the reaction of the silver ions with unknown plant biomolecules may involve protein catalysts and plant metabolites.<sup>[8]</sup> Those species may stimulate the AgNPs stabilization at lower extract concentrations but inhibit the AgNPs formation at higher concentrations.

The formation of AgNPs in radish extract solution was favored at higher pHs (see Figure 1f). Optimum conditions were achieved at pH 11.4, with a blue-shifted SPR band almost two-fold sharper than the other syntheses (see Table S3), revealing particles with smaller mean size and narrower size distribution. As discussed before, the hydroxyl groups can improve the reaction rate by forming reactive species, such as  $\text{Ag}_2\text{O}$  and others from the extract. Indeed, UV-Vis spectra presented in Figure S8 evidence those reactions after the irradiation of the extract at pH 11.4, leading to an intense absorption band centered at 274 nm, which disappears when the AgNPs are formed. These absorption bands can be associated with electronic transitions of carbonyls, flavonoids, aromatics and carboxylic compounds present in the honey and radish extracts.<sup>[36]</sup>

ATR-FTIR spectroscopy analyses after microwave irradiation on honey and radish-dried extracts without and with AgNPs were performed to identify the main functional groups and possible chemical changes. The ATR-FTIR spectra of honey and radish samples at different pHs are shown in Figure 2a and Figure 2b, respectively. Honey's spectra displayed a characteristic pattern of carbohydrates with peaks ranging from 1500 to

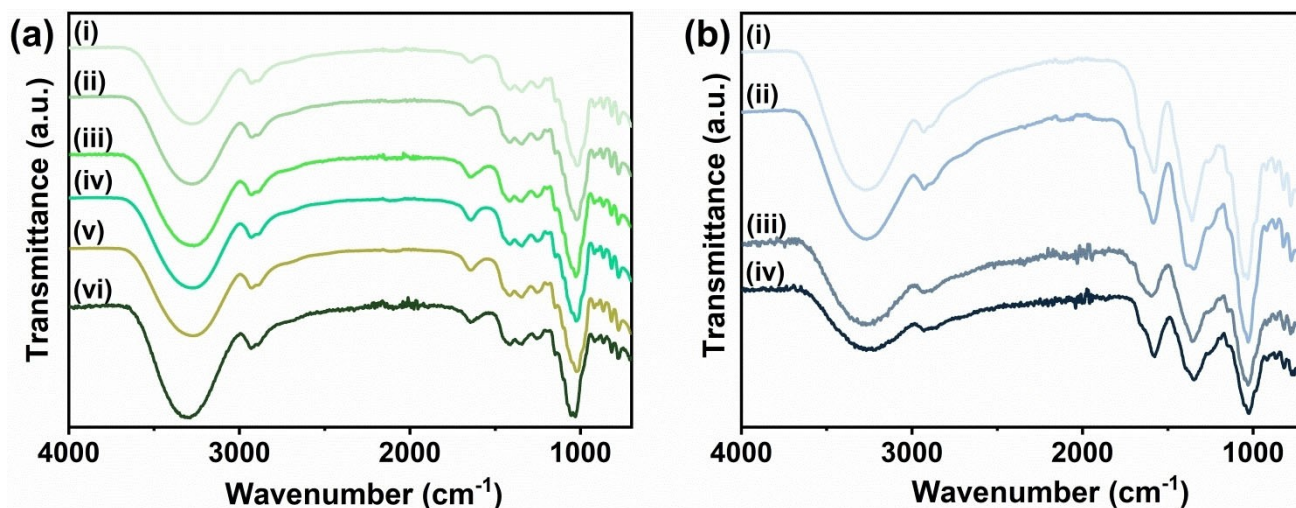


**Figure 2.** ATR-FTIR spectra of (a) honey dried solutions at pHs: (i) 3.8, (ii) 7, and (iii) 10 and AgNPs synthesized with honey at pHs: (iv) 3.8, (v) 7, (vi) 10; (b) radish dried extracts at pHs: (i) 6.5 and (ii) 11 and AgNPs synthesized with radish extract at pHs: (iii) 6.5 and (iv) 11.

800  $\text{cm}^{-1}$ , addressing to CO, C–OH, O–CH, and C–CH stretching vibrations<sup>[37]</sup> (Table S4). These FTIR patterns were expected since honey composition is constituted of 80–85% of carbohydrates, mainly from glucose and fructose.<sup>[9]</sup> The band at 3280  $\text{cm}^{-1}$  was attributed to O–H stretching, possibly from water/sugar molecules, while 2928 and 2883  $\text{cm}^{-1}$  peaks may be related to  $-\text{CH}_2$  stretching and rocking, respectively, from cellulose and lipids present in honey. Water also presented the symmetrical bending band at 1642  $\text{cm}^{-1}$ .<sup>[37]</sup> The FTIR spectra of the AgNPs exhibited similar band positions as that of pure honey (See Figure S9). It suggests that during the AgNPs synthesis there were no significant chemical changes, possibly due to the low concentration of  $\text{Ag}^+$  (i.e., 3  $\text{mmol L}^{-1}$ ). Slight shifts to greater wavenumbers of the band at  $\sim 1020 \text{ cm}^{-1}$ , attributed to  $\nu(\text{CO}) + \nu(\text{C–C})$  of carbohydrates, were observed when the pH of the honey solution was increased from 3.8 to 10. These shifts can be assigned to changes in gluconic acid molecules present in honey, as well as structural changes in fructose.

It is well known that sugars, like glucose, can act as reducing agents to produce AgNPs. Philip et al. found that fructose can act as a strong reducing agent.<sup>[10]</sup> One hypothesis is that reducing sugars (i.e. glucose, fructose) are responsible for the reduction of  $\text{Ag}^+$  cations, while stabilization may occur through sugars, as well as proteins, interaction with the AgNPs surface. Peaks related to amino acids (i.e., N–H) were not detected in honey samples; even though references indicate their presence.<sup>[38]</sup> Band overlapping could be responsible for the absence of their characteristic vibrations. Moreover, it indicates that the protein content in honey is low, matching the previous report of honey protein content (0.1–0.4%).<sup>[9]</sup> However, it has been stated that molecules such as carboxylates and amino acids present in honey may play an important role in AgNPs stabilization.<sup>[38]</sup>

The presence of water, carbohydrates, proteins, lipids as well as aromatic compounds have been previously identified in radish.<sup>[39]</sup> For the radish samples (Figure 2b), the peak located at

3270  $\text{cm}^{-1}$  is attributed to OH stretching of water/alcohol groups in carbohydrates or carboxylic acids, and N–H stretching of proteins<sup>[40]</sup> (Table S5). The 2932 and 2889  $\text{cm}^{-1}$  vibrations indicate the presence of  $\nu(\text{C–H})$  of lipids, while 1663  $\text{cm}^{-1}$  may be due to  $\delta(\text{OH}) + \nu(\text{C=O}) + \nu(\text{C–N})$  of proteins + aromatic ring vibrations.<sup>[39]</sup> In radish-dried extract at alkaline pH the peak attributed to  $\delta(\text{NH}) + \delta(\text{CN})$  of amide of proteins appeared at 1586  $\text{cm}^{-1}$ , while at neutral pH there was a shift to 1576  $\text{cm}^{-1}$ . Besides that, no expressive changes were seen on the vibrational spectra after AgNPs formation and at different pH (Figure S10).

TEM images of AgNPs synthesized using honey (Figure 3a,c,e) or radish extract (Figure 3b,d,f) show that all syntheses led to NPs with mean sizes smaller than 13 nm. The results of the obtained AgNPs employing honey solutions at different pHs demonstrated that there are no meaningful changes in the mean size between the samples, however, more aggregates were present at pH 7.0. Additional information regarding the crystal phase of the AgNPs was obtained by Fast Fourier Transform High-Resolution Transmission Electron Microscopy (FFT-HRTEM). The Figure 4 image shows that the NPs presented a face centered cubic (fcc) silver crystal structure. When the syntheses were carried out at pHs of 3.8 and 10.0 the same fcc crystal structure was obtained (Figures S11–12). The pH plays an important role in the formation and stabilization of the NPs synthesized with radish (compare Figure 3d and Figure 3f). The synthesis performed at pH 6.8 (Figure 3d) presented more agglomerated NPs, with a broader size distribution, where bigger particles can be observed. When the pH was raised to 11.4, well-distributed NPs were obtained, with a narrower size distribution and almost half in size. By varying the  $\text{AgNO}_3$  concentration (Figure 3b and Figure 3d), no significant changes in the mean size and size distributions were observed.

The stability of the AgNPs plays an important role in their application. Therefore, a series of runs were carried out to test

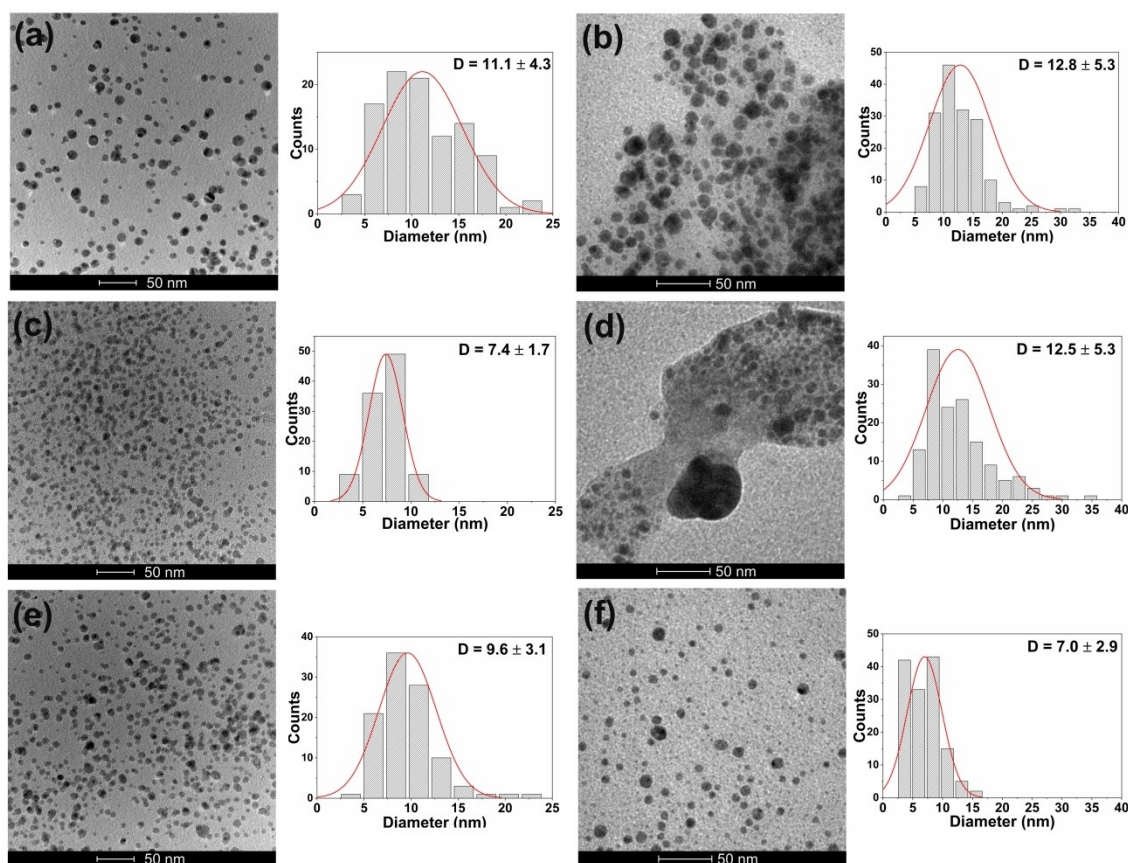


**Figure 3.** TEM images of AgNPs synthesized from honey or radish extract. [Honey] = 0.6 g mL<sup>-1</sup>, [AgNO<sub>3</sub>] = 3 mmol L<sup>-1</sup> at pHs: (a) 3.8, (c) 7.0 and (e) 10.0. [Radish extract] = 0.5 g mL<sup>-1</sup>: (b) [AgNO<sub>3</sub>] = 3 mmol L<sup>-1</sup> and pH 6.8, (d) [AgNO<sub>3</sub>] = 4.5 mmol L<sup>-1</sup> and pH 6.8, (f) [AgNO<sub>3</sub>] = 4.5 mmol L<sup>-1</sup> and pH 11.4.

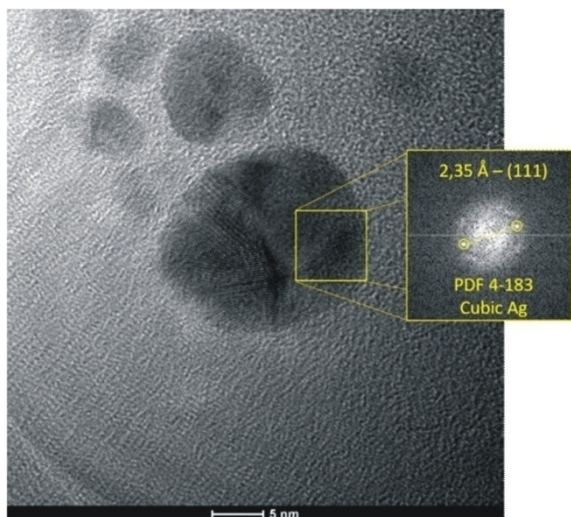


**Figure 4.** Typical FFT-HRTEM of AgNPs synthesized using [honey] = 0.6 g mL<sup>-1</sup>, [AgNO<sub>3</sub>] = 3 mmol L<sup>-1</sup> and pH 7.

their aging. The results showed high stability of the prepared AgNPs using honey (Figure 5a) and radish extract (Figure 5b). When radish extract was used, aggregation of NPs or dissolution of silver ions seems not to affect to a great extent the optical properties of the AgNPs SPR band. The  $\lambda_{\max}$  of

absorption remained constant after 120 days of aging and the intensity decreased by about 5% in the same period. When honey was used for the AgNPs synthesis the optical SPR changes are evident (see Figure 5a). The  $\lambda_{\max}$  of absorption remained constant in a similar behavior observed when radish extract was employed, but the intensity decreased by about 8% in the first week and 53.2% after 120 days.

In a typical investigation of photocatalytic hydrogen generation, the time evolution profiles correspond to several hours and the tests for reusability generally run for tens of hours. Additionally, when AgNPs are used as co-catalyst in hydrogen photocatalytic evolution experiments, a calcination step at 400 °C is previously carried out, thus the long-term stability of the AgNPs is not too crucial for the photocatalytic tests. For that reason, the AgNPs synthesized using honey were employed in the photocatalytic study of hydrogen evolution and the biosensor was built using AgNPs synthesized in radish extract medium. In this last case, a highly stable optical signal is required to avoid false positives during biodetection of extremely low concentrations of streptavidin and the AgNPs synthesized with radish were more appropriate.

To better understand the chemical states and stability of the AgNPs after microwave irradiation when honey was used for the synthesis, XPS analyses were carried out. Molecules such as carboxylates and amino acids are present in honey and they

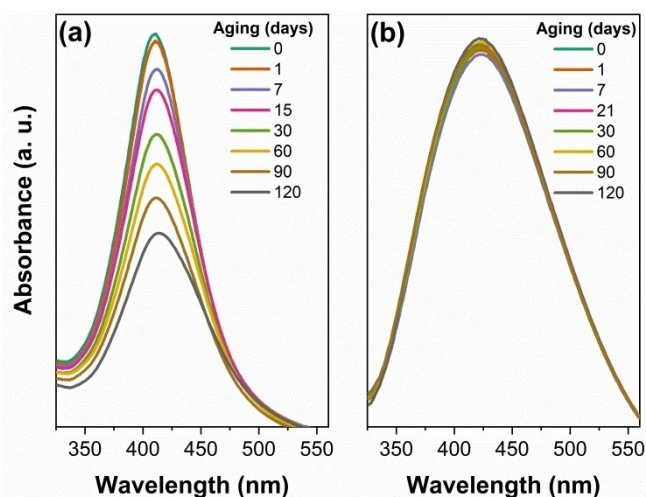


**Figure 5.** Aging of AgNPs synthesized using: (a) [honey] = 0.6 g mL<sup>-1</sup>, [AgNO<sub>3</sub>] = 3 mmol L<sup>-1</sup> and pH 3.8; (b) [radish] = 0.5 g mL<sup>-1</sup>, [AgNO<sub>3</sub>] = 4.5 mmol L<sup>-1</sup> and pH 6.8.

probably play an important role in AgNPs stabilization. The XPS survey spectrum of AgNPs did not show, as expected, the presence of silver (See Figure S13). The signals of C 1s, O 1s, and N 1s with relative concentrations of 83.6%, 15.4%, and 1.0% respectively are the main signals of the spectrum. Therefore, a series of XPS spectra were recorded after successive Ar<sup>+</sup> sputtering of the sample and the results are shown in Figure 6. After 10 min of sputtering two prominent peaks

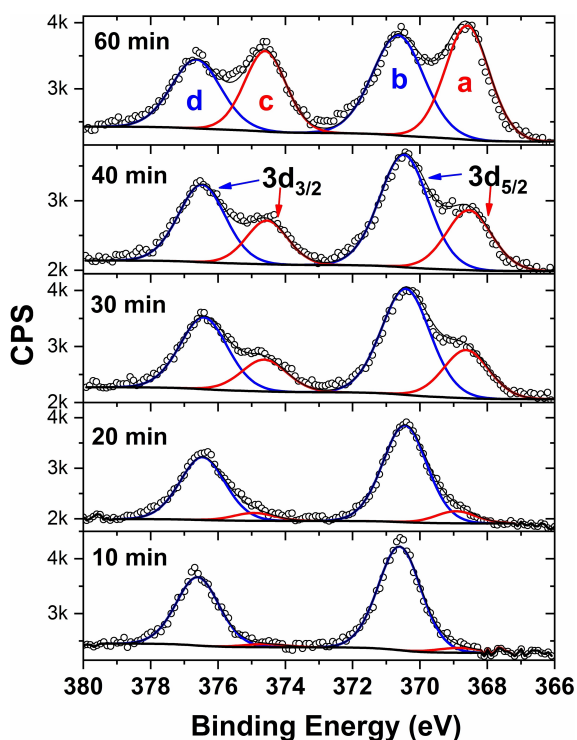


**Figure 6.** XPS spectra for the Ag 3d regions after sputtering of AgNPs synthesized using [honey] = 0.6 g mL<sup>-1</sup>, [AgNO<sub>3</sub>] = 6 mmol L<sup>-1</sup> and pH 3.8. The sputtering time is informed in the figure. Labels: a-d see text for details.

assigned to Ag 3d<sub>3/2</sub> and Ag 3d<sub>5/2</sub> levels appeared. The binding energy of Ag 3d core levels shifted towards higher binding energy values to that of the Ag metallic state and they are seen in Figure 6 (labels b and d). The calibration was carefully carried out after deconvolution of the C 1s signal for each sputtering series. In all the cases shown in Figure 6, the C–C–H signal at 285.0 eV was used as a reference. When the sputtering time increased from 10 min to 60 min two additional signals merged continually with the increase in sputtering time. These second XPS signals were already present at 10 min of sputtering but with a very low count rate (see Figure 6 bottom). The Ag 3d<sub>5/2</sub> (368.5 eV) and Ag 3d<sub>3/2</sub> (374.5 eV) signals, label a and c in Figure 6 respectively, may be assigned to Ag (0), with a splitting of 6.0 eV.<sup>[41]</sup> The Ag 3d<sub>5/2</sub> binding energies of metallic silver and its oxides have been investigated in detail in the past and the dispersion or even superposition of binding energies reveal that their assignments are not trivial. Ferraria, A. M. et al. have reinvestigated the XPS signals of Ag and its salts including Auger spectroscopy data of Ag MNN signals in a very thorough work.<sup>[42]</sup> They found that the Ag 3d<sub>5/2</sub> was reported from 367.9 to 368.4 eV ( $\Delta = 0.5$  eV) for metal Ag; from 367.6 to 368.5 eV ( $\Delta = 0.9$  eV) for Ag<sub>2</sub>O and from 367.3 to 368.1 eV ( $\Delta = 0.8$  eV) for AgO. The maximum difference in the binding energies of the above numbers, independent of the oxidation state of the silver, is 1.2 eV. Additional works have also reported results within the energy range of 1.2 eV.<sup>[43–48]</sup> Ferraria, A. M. et al. concluded that Ag(0) can be distinguished from oxidized Ag species mainly through the Auger parameters. They also reported that the Ag(I) 3d in AgO has about 0.4 eV lower binding energy than the Ag(I) 3d in Ag<sub>2</sub>O. Nevertheless, all the above reports, the energy difference of the Ag 3d<sub>5/2</sub> signals a–b in Figure 6 is 2 eV (a: 368.5 ± 0.1 eV; b: 370.5 ± 0.2 eV). Similarly, the difference of the Ag 3d<sub>3/2</sub> signals c–d in Figure 6 is 1.9 eV (c: 374.6 ± 0.1 eV; d: 376.50 ± 0.2 eV). A difference of about 2 eV between the Ag 3d duplets means that only different oxidations states cannot explain the results presented in Figure 6. Moreover, the FWHM of the Ag 3d signals deconvoluted in Figure 6 are between 1.4 eV and below 1.8 eV. The XPS system does not have a monochromator and the addition of new synthetic signals in the data treatment would produce artificial artifacts.

Systematic works have also been reported on AgNPs XPS data aiming to identify the contribution of size and chemical effects from the measured binding energies of the Ag core electrons. For instance, Shin, H. S et al. have prepared AgNPs by  $\gamma$ -radiation in an aqueous solution of AgNO<sub>3</sub>, isopropanol, and polyvinyl pyrrolidone.<sup>[43]</sup> The average diameters of the as-prepared AgNPs were 12.1 nm and 19.6 nm when the NPs were prepared from 0.01 and 0.5 mol L<sup>-1</sup> AgNO<sub>3</sub> solutions, respectively. The formation of NPs between 3 and 6 nm in diameter were also abundant. The Ag 3d<sub>5/2</sub> signals of the AgNPs core electrons were found to increase with the decrease in the nanoparticle size. Additionally, the binding energy shifted to lower energies from 1.4 eV to 0.5 eV before and after sputtering respectively. Lopez-Salido L. et al. studied the growth of noble metal NPs on mildly sputtered and non-sputtered highly ordered pyrolytic graphite or WSe<sub>2</sub> surfaces.<sup>[49]</sup> AgNPs were grown by evaporating a silver rod under UHV conditions and

the diameter and high of the NPs were precisely measured by scanning tunnelling microscopy (STM). XPS results showed that the Ag3d states converged to the bulk properties at much larger particles size than 6 nm in diameter and 5 nm in height. The authors attributed that phenomenon to either inefficient final state screening, difference in particle geometry or both effects together. In addition, the XPS signal was strongly depended on the interaction Ag-oxide metal substrate. The results presented in Figure 6 can be interpreted taking into account the presence of different AgNPs sizes contributions. In the present work, the size of the prepared AgNPs ranged from less than 6 nm to more than 15 nm (see Figure 3 a, c and d). The sputtering conditions of the present work were much more aggressive in energy, time, and current than the study carried out by Lopez-Salido L. et. al.<sup>[49]</sup> Therefore, it is hypothesized that the strong sputtering conditions used here quickly eliminated the main proteins capping agents of the AgNPs together with the smaller NPs. However, a probable diffusion of the smaller stabilized AgNPs during solvent evaporation for the preparation of the samples for XPS analyses cannot be ruled out.

### Green AgNPs applications: hydrogen photogeneration and nanoplasmonic biosensing

Pristine TiO<sub>2</sub> NPs synthesized by a microwave-assisted methodology using Titanium (IV) bis (ammonium lactato) dihydroxide solution as the titanium precursor, were impregnated with AgNPs prepared using honey solutions as stabilizing and reducing medium. The optical properties of TiO<sub>2</sub> NPs and TiO<sub>2</sub>@AgNPs were investigated using DRS UV-Vis (Figure S14a). The impregnation of AgNPs as co-catalyst led to almost no apparent change in the bandgap, of about 3.15 eV, compared to pristine TiO<sub>2</sub> NPs. By taking a closer look at the 1.55–3.2 eV region, an absorption band can be observed (Figure S14b), which is attributed to the presence of AgNPs on the surface of the TiO<sub>2</sub> NPs. Figure 7a shows a typical hydrogen evolution on

pristine TiO<sub>2</sub> NPs and TiO<sub>2</sub>@AgNPs under UV-vis and only visible light irradiation ( $\geq 400$  nm). Hydrogen generation evolves steadily under UV-vis and also under only visible light irradiation (Figure 7a). The rate of hydrogen generation on TiO<sub>2</sub>@AgNPs photocatalyst under visible light is much lower than UV-vis illumination, but shows the potential of the photocatalyst to be active also under visible light irradiation. On the contrary, TiO<sub>2</sub> NPs did not show any activity under visible light irradiation. TiO<sub>2</sub>@AgNPs hydrogen evolution rate under UV-vis irradiation was 3.5 x greater than pristine TiO<sub>2</sub> NPs, showing again the high potential of the prepared green TiO<sub>2</sub>@AgNPs photocatalyst for solar to hydrogen conversion. Additionally, the TiO<sub>2</sub>@AgNPs showed excellent recycling properties that led to a constant generation of hydrogen in three consecutive photocatalytic cycles (see Figure 7b).

To get insight into the photocatalyst surface modifications due to the presence of the reactive medium, Ag 3d XPS spectra were obtained before and after photolysis for the TiO<sub>2</sub>@AgNPs (Figure S15). Fresh TiO<sub>2</sub>@AgNPs spectrum demonstrated that the Ag species corresponded to an oxidized phase (AgO or Ag<sub>2</sub>O), with Ag 3d<sub>5/2</sub> and Ag 3d<sub>3/2</sub> peaks binding energies of 367.9 eV and 373.8 eV, respectively. After three runs of photolysis, slight shifts of the Ag 3d<sub>5/2</sub> and Ag 3d<sub>3/2</sub> peaks were observed, to 367.4 eV and 373.3 eV, respectively (Figure S15). Due to the energy resolution of the XPS equipment, it is not possible to infer that the Ag species became more oxidized after UV-vis irradiation. In all the cases, the XPS spectra had the Ag 3d doublet splitting of  $\sim 5.9$  eV.

The plasmonic sensing ability from AgNPs films obtained with radish extracts was first tested by monitoring the plasmonic band (inset in Figure 8a) when immersing the films in glucose solutions with different concentrations (refractive index ranging from  $\sim 1.335$  to  $\sim 1.348$ ). The SPR band red-shifted by about 3 nm, resulting in a bulk sensitivity of about 201 nm RIU<sup>-1</sup> (RIU: refractive index unit) which is ca. 30% higher than the LSPR sensitivities from AgNPs synthesized with conventional methods in films (see Table S6).

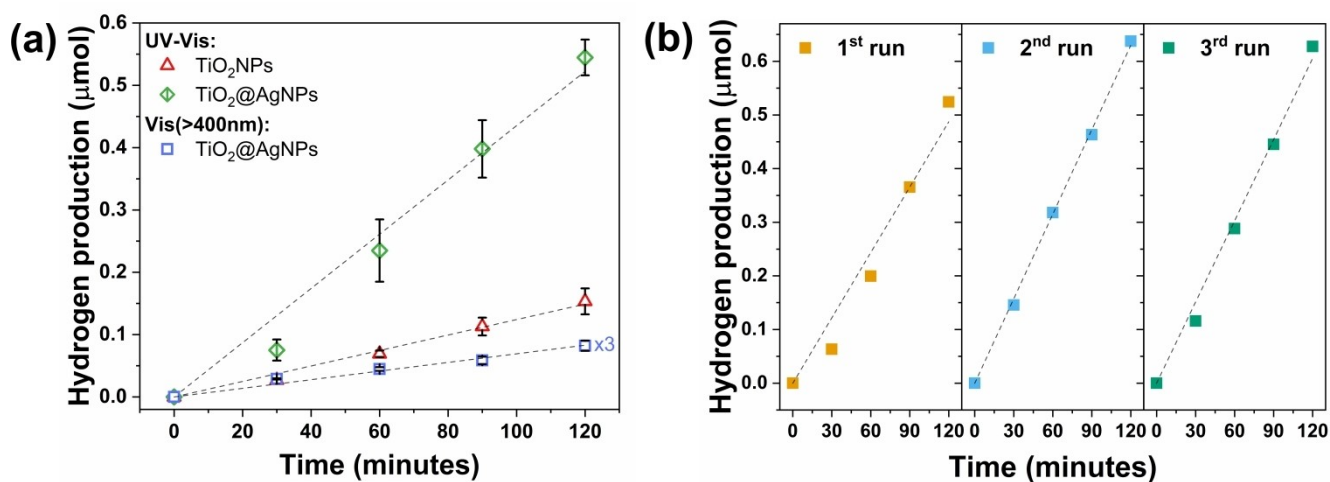


**Figure 7.** (a) Hydrogen photogeneration experiments under UV-vis and visible radiation using the pristine TiO<sub>2</sub> and TiO<sub>2</sub>@AgNPs. (b) Recycling of TiO<sub>2</sub>@AgNPs photocatalyst under UV-Vis irradiation during 3 cycles. In all cases methanol was used as sacrificial agent (methanol/water  $\sim 1/8$  v/v) and the AgNPs were synthesized using [honey] = 0.6 g mL<sup>-1</sup>, [AgNO<sub>3</sub>] = 6 mmol L<sup>-1</sup> and pH 3.8.

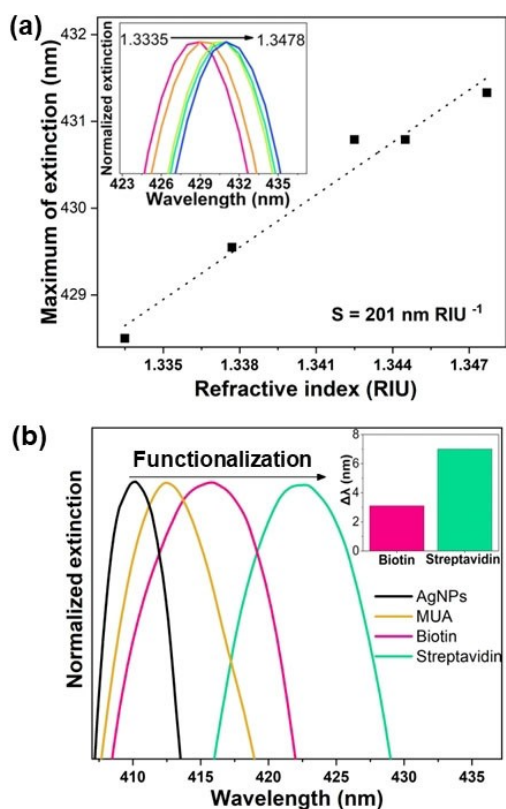


**Figure 8.** (a) Sensitivity of AgNPs nanoplasmonic multilayer film for biosensing using glucose solutions; (b) SPR shift for AgNPs functionalization with 11-mercaptoundecanoic acid (MUA), followed by the adsorption of biotin and streptavidin.

Nanoplasmonic biosensors were assembled using AgNPs functionalized with biotin for biorecognition of streptavidin in PBS solution. Biotin participates in a wide range of metabolic processes where it attaches covalently to proteins, nucleic acids, or other molecules. Streptavidin is a tetrameric protein that also links to antibodies, inhibitors, and nucleic acids with minimal impact on its biological activity. The biotin–streptavidin system has a high affinity constant ( $K \sim 10^{13} \text{ molL}^{-1}$ ), turning out to be an appropriate receptor-analyte model to demonstrate the biosensor performance.<sup>[50,51]</sup> Figure 8b shows the results of protein binding experiments. The wavelength red shifts ( $\Delta\lambda$ ) were calculated using the LSPR absorption band of 11-mercaptoundecanoic acid (MUA) as reference and plotted in the inset of Figure 8b. The total surface assembly MUA-biotin-streptavidin ( $0.125 \text{ mg mL}^{-1}$ ) corresponded to a  $\Delta\lambda$  of about 12 nm, resulting from the increase in the localized refractive index near the AgNPs surface with the molecular bindings. Therefore, green AgNPs can be applied as substrates for plasmonic biosensing. Through their functionalization with the biorecognition element (in this case biotin), the analyte (streptavidin) could be detected. The same setup may be employed for different types of biodetection, such as antibody-antigen, enzyme-protein, etc.

In conventional synthesized methods of AgNPs films shifts of about 7 nm were observed (streptavidin  $50 \mu\text{g mL}^{-1}$ ), lower than the present method. The wavelength red shifts ( $\Delta\lambda$ ) were

calculated using the SPR absorption band of MUA as reference (inset of Figure 8b). The total surface assembly (MUA-biotin-streptavidin) corresponded to a  $\Delta\lambda$  of about 12 nm showing a small increase in the surface-average refractive index at or near the AgNPs surface; but enough to detect analyte binding at very low concentrations.

## Conclusions

This work shows a new and affordable method for AgNPs synthesis using natural extracts from food (honey and radish) and a green heating source (microwave irradiation). This method is eco-friendly and non-toxic. The methodology employed here also showed that AgNPs could be formed by microwave irradiation of extracts obtained from the skin or rotten radish. The investigation unveiled a strong dependence on nucleation, stabilization, and therefore on the growth and coalescence mechanism with the chemical composition of the natural extract used during the synthesis. As result, the concentrations of silver precursor and natural extract, in addition to pH had different impacts on the growth mechanism of the nanoparticles. In general, AgNPs with mean diameters smaller than 13 nm were obtained. The AgNPs presented high stability as the  $\lambda_{\text{max}}$  of absorption remained constant after 120 days of aging (for both extracts). However, when honey was used as medium for the synthesis the  $\lambda_{\text{max}}$  of absorption also remained constant, but the intensity decreased along the aging days.

The prepared green AgNPs were impregnated onto  $\text{TiO}_2$  NPs ( $\text{TiO}_2/\text{AgNPs}$ ) and used for hydrogen generation in the photo-reform of methanol at room temperature. The hydrogen evolution was stable, even under only visible light irradiation, and showed excellent recycling properties. In a second application, it was assembled a chip with a film of the AgNPs, presenting a LSPR sensitivity of  $201 \text{ nm RIU}^{-1}$ . Finally, the AgNPs chip was applied as a nanoplasmonic biosensor to estimate the potential of detecting biomarkers using biotin and streptavidin as a model system. The surface assembly was enough to detect analyte binding at extremely low concentrations with a total redshift ( $\Delta\lambda$ ) of about 12 nm. This work highlights that the green synthesis of AgNPs using microwave irradiation and only honey or radish extracts as reducing and stabilizing agents provides environmentally friendly approaches at low cost and scalable for the synthesis of silver nanoparticles.

## Experimental Section

### Materials

Honey and fresh pink radish (*Raphanus sativus*) were obtained from local customers (Porto Alegre, RS – Brazil). Silver nitrate ( $\text{AgNO}_3$ ) was purchased from Plat LAB, Brazil. Titanium (IV) bis (ammonium lactate) dihydroxide solution (TALH), 50 wt.% in  $\text{H}_2\text{O}$ , ammonium hydroxide, sodium hydroxide (NaOH), 3-mercaptopropyl trimethoxysilane (MPTMS), D-(+)-glucose, 11-mercaptoundecanoic acid (MUA), N-ethyl-N-(3-dietilaminepropyl carbodiimide) (EDC), N-hy-



droxisuccinimide (NHS), biotin, dimethyl sulfoxide (DMSO), and streptavidin p.a. were acquired from Sigma-Aldrich. Sulfuric acid ( $\text{H}_2\text{SO}_4$ ) was purchased from Vetec Química Fina Ltda. Hydrogen peroxide ( $\text{H}_2\text{O}_2$ ), ethanol, methanol, and nitric acid ( $\text{HNO}_3$ ) were obtained from Casa da Química.  $0.1 \text{ mol L}^{-1}$  (pH 7) phosphate buffer solution (PBS) was prepared using sodium phosphate monobasic monohydrate ( $\text{NaH}_2\text{PO}_4$ ) and sodium phosphate dibasic ( $\text{Na}_2\text{HPO}_4$ ) both acquired from Sigma-Aldrich.

### Preparation of honey solutions

Aqueous honey solutions were prepared by mixing different concentrations of honey with ultrapure water (milli-Q®). The concentration of these solutions varied between  $0.1$  and  $1.0 \text{ g mL}^{-1}$  weight of honey (g) per mL of ultrapure water. The mixtures were sonicated for 30 minutes prior to the AgNPs syntheses.

### Preparation of radish extract solutions

For the preparation of aqueous radish extract solutions, the vegetable (*Raphanus sativus*) was washed with tap water, peeled, washed with deionized water, and finally dried with filter paper. Radish roots or their peel were blended in a Philips kitchen blender (600 W) with ultrapure water until homogenization. Radish root extract concentrations varied between  $0.25$  and  $2 \text{ g mL}^{-1}$  – weight of radish root (g) per mL of ultrapure water. Finally, the obtained mixtures were vacuum filtered, using G2 and G4 sintered glass filters, and the filtered solutions were used.

### Synthesis of Silver nanoparticles

Silver nanoparticles (AgNPs) syntheses were conducted using aqueous honey or radish extract solutions (final volume of  $30 \text{ mL}$ ) and  $\text{AgNO}_3$  as the silver precursor ( $0.50 \text{ mol L}^{-1}$ ). The desired volume of the  $\text{AgNO}_3$  solution was added to the honey/radish extract solutions using a micropipette, under vigorous stirring, and introduced to a homemade Teflon reactor. The final AgNPs were obtained after irradiating the sample for 30 seconds at maximum power in a commercial Panasonic Microwave oven (1600 W). The optical properties were investigated by changing the synthesis conditions (concentration of honey/radish extract solutions;  $\text{AgNO}_3$  concentration; and pH (modified with  $\text{NaOH}$  or  $\text{HNO}_3$ )).

### Impregnation of $\text{TiO}_2$ NPs with AgNPs.

$\text{TiO}_2$  nanoparticles ( $\text{TiO}_2$  NPs) were impregnated with AgNPs synthesized using a honey solution ( $[\text{honey}] = 0.6 \text{ g mL}^{-1}$ ;  $[\text{AgNO}_3] = 6 \text{ mmol L}^{-1}$ ; pH 3.8. Before the impregnation, the AgNPs were centrifuged at  $14,000 \text{ rpm}$  for  $10 \text{ min}$  and only the supernatant was used forward. The impregnation procedure was done by a modified wet impregnation method, consisting of the dispersion of the  $\text{TiO}_2$  NPs into ultrapure water, by stirring and sonication during  $1 \text{ hour}$ , followed by the addition of the colloidal AgNPs. The mixture was stirred and sonicated for  $1 \text{ hour}$  and rested overnight aiming for the adsorption equilibrium of the AgNPs onto the  $\text{TiO}_2$  NPs surface. The supernatant was removed, and the precipitate was oven-dried at  $80^\circ\text{C}$  for  $12 \text{ h}$ . Finally, it was calcined at  $400^\circ\text{C}$  for  $3 \text{ h}$ , with a heating rate of  $5^\circ\text{C}$  per minute. Pristine  $\text{TiO}_2$  NPs were also synthesized by a MW assisted methodology, using an aqueous ammoniacal solution and TALH as the titanium precursor. Briefly,  $5 \text{ mL}$  of TALH was mixed with  $45 \text{ mL}$  of  $0.1 \text{ mol L}^{-1}$  of  $\text{NH}_3$  and irradiated for  $15 \text{ min}$  at  $160^\circ\text{C}$  using a Microwave Digestion System MARS 6 (CEM Corporation). The detailed procedure is reported on a previous work of our research group.<sup>[52]</sup>

### Photocatalytic measurements

Hydrogen photogeneration experiments were performed using a Teflon reactor of ( $24.16 \pm 0.01$ ) mL, with a quartz window of  $2.54 \text{ cm}$  in diameter. Methanol was used as sacrificial agent with a methanol/water solution proportion of  $\sim 1/8 \text{ v/v}$ . Photogeneration experiments were carried out by the dispersion of the photocatalyst ( $1 \text{ mg mL}^{-1}$ ) in the methanol/water solution, followed by its sonication during 30 minutes. The reactor was deaerated with nitrogen for 30 minutes prior to irradiation. A high-pressure Xe/Hg lamp (350 W, Scientech) was used for the photolysis, allowing the irradiation of the samples under a wide spectral range. Visible light experiments were performed using a Long Wave Pass Filter,  $25.4 \text{ mm}$ ,  $400 \pm 5 \text{ nm}$  cut-on ( $-1200 \text{ nm}$ ) from Newport. Gas chromatography (Shimadzu GC-2010) was used to evaluate the photocatalytic activity, using a molecular sieve 5 A packed column, following a procedure previously reported.<sup>[53,54]</sup>

### Preparation of nanoplasmonic biosensors

The following cleaning and adsorption methodologies were adapted from previous works. Microscopy glass slides, with  $2 \text{ cm}^2$  of area ( $2.5 \text{ cm} \times 0.8 \text{ cm}$ ), were cleaned by its sequential submersion on ethanol, acetone, deionised water, and piranha solution ( $\text{H}_2\text{O}_2/\text{H}_2\text{SO}_4$  1/3 in volume), respectively, and finally washed with deionised water. Next, the slides were immersed in an ethanol solution of MPTMS ( $10 \text{ mmol L}^{-1}$ ) for  $24 \text{ h}$ , maintaining at  $60^\circ\text{C}$  for the first  $2 \text{ h}$  and at room temperature for  $22 \text{ h}$ . To remove any excess of MPTMS, the slides were washed with ethanol and deionised water. A  $2 \text{ h}$  curing process at  $120^\circ\text{C}$  was done to improve AgNPs adsorption, followed by the immersion of the slides on the colloidal AgNPs ( $[\text{radish extract}] = 0.5 \text{ g mL}^{-1}$ ;  $[\text{AgNO}_3] = 4.5 \text{ mmol L}^{-1}$ ; pH 11.4) for  $48 \text{ h}$ . A second deposition of AgNPs was done onto the slides by dipping them into a solution containing  $300 \mu\text{L}$  of MPTMS and  $250 \mu\text{L}$  of  $0.1 \text{ mol L}^{-1}$  HCl in  $25 \text{ mL}$ , followed by immersion into the colloidal AgNPs for  $1 \text{ h}$ . The subsequent AgNPs layers were adsorbed by following the same procedure. Protein detection via LSPR involves a series of steps related to the surface of the AgNPs film. For the formation of the label free nanoplasmonic biosensor, the methodology proposed by Peixoto et al. was used.<sup>[23]</sup> First, the substrate with one layer of AgNPs was placed on an ethanol solution of  $1 \text{ mmol L}^{-1}$  of MUA for  $72 \text{ h}$  (MUA has a thiol group, which covalently binds to AgNPs). The slide was washed with ethanol, followed by deionised water, and placed in a 1:1 solution of EDC/NHS  $0.1 \text{ mol L}^{-1}$  for  $3 \text{ h}$ . The modified substrate was immersed in a  $6 \text{ mg mL}^{-1}$  biotin solution of in DMSO for  $6 \text{ h}$ . After that procedure, the substrate was ready to interact with streptavidin and was immersed on a PBS solution containing  $0.125 \text{ mg mL}^{-1}$  of this protein for  $15 \text{ minutes}$ .

### Characterization

UV-vis spectroscopy studies were performed on the colloidal AgNPs to follow their formation and to investigate their mean size, size distribution and stability over time. Spectra were obtained in the wavelength range of  $200\text{--}800 \text{ nm}$ , using a CARY 50 spectrophotometer (Varian). A double-beam CARY 5000 spectrophotometer (Varian) was used to follow the AgNPs film formation, after each deposition procedure. The measurements were performed with the slide immersed in distilled water, using a baseline of the slide only with MPTMS, also immersed in distilled water. The functionalization of the AgNPs slide was also accompanied by UV-Vis spectroscopy, but now immersed on PBS pH 7. The sensitivity of the AgNPs multilayer film was determined by acquiring UV-Vis spectra in solutions with increasing refractive indexes. Aqueous solutions with different D-(+)-glucose concentrations (from  $0$  to  $100 \text{ mg mL}^{-1}$ )

resulted in refractive indexes ranging from 1.3350 to 1.3477 RIU (refractive index unit). Refractive index changes were determined by an ATAGO 4410 digital refractometer. The optical properties of the pristine TiO<sub>2</sub> NPs and TiO<sub>2</sub> NPs impregnated with AgNPs (TiO<sub>2</sub>@AgNPs) were measured using the same equipment. The Kubelka–Munk equation was employed to analyse the data, assuming that the sample scattering coefficient was constant for the UV–Vis wavelength range. All measurements were done in the wavelength range of 200–800 nm. To identify the main functional groups of aqueous honey and radish extract solutions under different pHs, attenuated total reflectance infrared spectroscopy (ATR-FTIR) measurements were conducted using an Alpha-Bruker equipment, with infrared source ranging from 500 to 4000 cm<sup>-1</sup> and 4 cm<sup>-1</sup> resolution. Samples were prepared by oven drying the solutions and the as synthesized colloidal AgNPs at ~80 °C overnight.

Transmission electron microscopy (TEM) was used to determine the mean size and morphology of the AgNPs. TECNAI G2 and FEI TECNAI F20 (Netherlands) microscopes operating at 200 kV were used to perform the measurements. For some TEM measurements the FEI microscope model Morgagni 268D was also used. The mean size of the NPs was measured using the software ImageJ®. X-ray photoelectron spectroscopy (XPS) was used to confirm the presence of silver in the synthesized NPs and in order to determine its chemical state. XPS measurements were carried out using a Mg K $\alpha$  (1253.6 eV) source and a conventional electron spectrometer (Omicron GmbH, Germany) equipped with a high-performance hemispherical energy analyzer and a seven-channeltron detector. Surveys spectra were obtained with a pass energy of 50 eV, while the selected atomic signals were acquired with 10 or 30 eV. Casa XPS software package was used to deconvolute the obtained spectra. All the measured spectra were corrected by setting the reference binding energy of carbon (C 1s) at 285.0 eV. Spectra single atom fittings were carried out using a mixed Gauss-Lorentz function and a Shirley background. The AgNPs sample used on XPS measurements was prepared by the dispersion of colloidal AgNPs on ethanol–1:4 AgNPs:ethanol (v/v) – followed by its centrifugation at 14,000 rpm. After the removal of the supernatant, the precipitate was rinsed with distilled water multiple times and oven dried at ~100 °C for 2 hours. XPS spectra were also obtained after sputtering of the AgNPs sample. A 5 keV Argon ion beam was used in situ in the analysis chamber maintaining a constant argon pressure of 8.0 × 10<sup>-8</sup> mbar during sputtering. The ion current and time period of sputtering was 3 mA and 60 min respectively.

## Acknowledgements

This work was funded in part by Fundação de Amparo à Pesquisa do Estado de São Paulo (FAPESP CEPID-finance code 2013/07296-2), Conselho Nacional de Desenvolvimento Científico e Tecnológico-CNPq (finance codes 166281/2017-4 and 305048/2022-8), Coordenação de Aperfeiçoamento de Pessoal de Nível Superior-CAPES (finance code 001), Fundação de Amparo à Pesquisa do Estado do Rio Grande do Sul (FAPERGS 23/2551-0000504-2) and Centro de Tecnologias Estratégicas do Nordeste (CETENE). M.A. was supported by the Margarita Salas postdoctoral contract MGS/2021/21 (UP2021-021) financed by the European Union-Next Generation EU.

## Conflict of Interests

The authors declare no conflict of interest.

## Data Availability Statement

The data that support the findings of this study are available from the corresponding author upon reasonable request.

**Keywords:** Honey · radish extract · hydrogen · microwave · nanoplasmonic biosensor

- [1] C. Vanlalveni, S. Lallianrawna, A. Biswas, M. Selvaraj, B. Changmai, S. L. Rokhum, *RSC Adv.* **2021**, *11*, 2804–2837.
- [2] X. Wang, L. Yuan, H. Deng, Z. Zhang, *Food Chem.* **2021**, *338*, 127807.
- [3] I. Jahan, F. Erci, I. Isildak, *Anal. Lett.* **2019**, *52*, 1860–1873.
- [4] H. M. Mehwish, M. S. R. Rajoka, Y. Xiong, H. Cai, R. M. Aadil, Q. Mahmood, Z. He, Q. Zhu, *J. Environ. Chem. Eng.* **2021**, *9*, 105290.
- [5] K. T. Hassan, I. J. Ibraheem, O. M. Hassan, A. S. Obaid, H. H. Ali, T. A. Salih, M. S. Kadhim, *J. Environ. Chem. Eng.* **2021**, *9*, 105359.
- [6] M. Khan, M. R. Shaik, S. F. Adil, S. T. Khan, A. Al-Warthan, M. R. H. Siddiqui, M. N. Tahir, W. Tremel, *Dalton Trans.* **2018**, *47*, 11988–12010.
- [7] T. Dutta, N. N. Ghosh, M. Das, R. Adhikary, V. Mandal, A. P. Chattopadhyay, *J. Environ. Chem. Eng.* **2020**, *8*, 104019.
- [8] M. Ali, B. Kim, K. D. Belfield, D. Norman, M. Brennan, G. S. Ali, *Mater. Sci. Eng. C* **2016**, *58*, 359–365.
- [9] E. R. Balasooriya, C. D. Jayasinghe, U. A. Jayawardena, R. W. D. Ruwanthika, R. M. De Silva, P. V. Udagama, *J. Nanomater.* **2017**, *2017*.
- [10] D. Philip, *Spectrochim. Acta Part A* **2009**, *73*, 650–653.
- [11] V. Snitka, D. Naumenko, L. Ramanauskaitė, S. A. Kravchenko, B. A. Snopok, *Theor. Exp. Chem.* **2011**, *47*, 296–302.
- [12] A. S. Kumar, G. Madhu, E. John, S. V. Kuttinarayanan, S. K. Nair, *Green Process. Synth.* **2020**, *9*, 268–274.
- [13] N. A. Ismail, K. Shameli, M. M. T. Wong, S. Y. Teow, J. Chew, S. Sukri, *Mater. Sci. Eng. C* **2019**, *104*.
- [14] P. B. Kane, P. Jagtap, R. D. Kale, A. R. Rao, *Adv. Nat. Sci. Nanosci. Nanotechnol.* **2019**, *10*.
- [15] R. Goyeneche, S. Roura, A. Ponce, A. Vega-Gálvez, I. Quispe-Fuentes, E. Uribe, K. Di Scala, *J. Funct. Foods* **2015**, *16*, 256–264.
- [16] Z. G. Xiao, L. Yue, C. X. Wang, F. R. Chen, Y. Ding, Y. L. Liu, X. S. Cao, Z. Chen, S. Rasmann, Z. Y. Wang, *J. Hazard. Mater.* **2021**, *411*.
- [17] D. Liu, L. Liu, L. Yao, X. Y. Peng, Y. Li, T. T. Jiang, H. Y. Kuang, *J. Drug Deliv Sci Technol* **2020**, *55*.
- [18] W. L. Zhang, Y. B. Dan, H. L. Shi, X. M. Ma, *ACS Sustainable Chem. Eng.* **2016**, *4*, 5424–5431.
- [19] P. R. Hanlon, D. M. Barnes, *J. Food Sci.* **2011**, *76*, C185–C192.
- [20] R. Goyeneche, S. Roura, A. Ponce, A. Vega-Gálvez, I. Quispe-Fuentes, E. Uribe, K. Di Scala, *J. Funct. Foods* **2015**, *16*, 256–264.
- [21] M. M. Momeni, M. Taghinejad, Y. Ghayeb, A. N. Chermahini, R. Bagheri, Z. Song, *Appl. Phys. A* **2021**, *127*, 104–104.
- [22] J. Zhao, X. Y. Zhang, C. R. Yonzon, A. J. Haes, R. P. Van Duyne, *Nanomedicine* **2006**, *1*, 219–228.
- [23] L. P. F. Peixoto, J. F. L. Santos, G. F. S. Andrade, *Anal. Chim. Acta* **2019**, *1084*, 71–77.
- [24] D. Karthiga, S. P. Anthony, *RSC Adv.* **2013**, *3*, 16765–16774.
- [25] M. R. Bindhu, M. Umadevi, G. A. Esmail, N. A. Al-Dhabi, M. V. Arasu, *J. Photochem. Photobiol. B, Biol.* **2020**, *205*, 111836.
- [26] V. Dal Lago, L. F. de Oliveira, K. D. Goncalves, J. Kobarg, M. B. Cardoso, *J. Mater. Chem.* **2011**, *21*, 12267–12273.
- [27] E. Turunc, O. Kahraman, R. Binzet, *Anal. Biochem.* **2021**, *621*.
- [28] K. Varghese Alex, P. Tamil Pavai, R. Rugmini, M. Shiva Prasad, K. Kamakshi, K. C. Sekhar, *ACS Omega* **2020**, *5*, 13123–13129.
- [29] J. Kadam, P. Dhawal, S. Barve, S. Kakodkar, *SN Appl. Sci.* **2020**, *2*, 738.
- [30] G. B. Strapasson, M. Assis, C. W. Backes, S. A. Corrêa, E. Longo, D. E. Weibel, *Int. J. Hydrogen Energy* **2021**, *46*, 34264–34275.
- [31] S. Wu, F. Wang, Q. Li, J. Wang, Y. Zhou, N. Duan, S. Niazi, Z. Wang, *Food Chem.* **2020**, *323*, 126823.
- [32] D. D. Evanoff Jr, G. Chumanov, *ChemPhysChem* **2005**, *6*, 1221–1231.

- [33] S. K. Mahapatra, K. A. Bogle, S. D. Dhole, V. N. Bhoraskar, *Nanotechnology* **2007**, *18*, 135602.
- [34] S. Nishimura, D. Mott, A. Takagaki, S. Maenosono, K. Ebitani, *Phys. Chem. Chem. Phys.* **2010**, *13*, 9335–9343.
- [35] P. S. Ramesh, T. Kokila, D. Geetha, *Spectrochim. Acta Part A* **2015**, *142*, 339–343.
- [36] E. H. Anouar, J. Gierschner, J.-L. Duroux, P. Trouillas, *Food Chem.* **2012**, *131*, 79–89.
- [37] J. Stojkovska, P. Petrovic, I. Jancic, M. T. Milenkovic, B. Obradovic, *Appl. Microbiol. Biotechnol.* **2019**, *103*, 8529–8543.
- [38] D. Philip, *Spectrochim. Acta Part A* **2010**, *75*, 1078–1081.
- [39] N. Zuverza-Mena, R. Armendariz, J. R. Peralta-Videa, J. L. Gardea-Torresdey, *Front. Plant Sci.* **2016**, *7*.
- [40] J. Osuntokun, D. C. Onwudiwe, E. E. Ebenso, *Green Chem. Lett. Rev.* **2019**, *12*, 444–457.
- [41] J. F. Moulder, *Handbook of X-ray Photoelectron Spectroscopy: A Reference Book of Standard Spectra for Identification and Interpretation of XPS Data*, Physical Electronics Division, Perkin-Elmer Corporation, USA, **1992**, p. 261..
- [42] A. M. Ferrara, A. P. Carapeto, A. M. Botelho do Rego, *Vacuum* **2012**, *86*, 1988–1991.
- [43] H. S. Shin, H. C. Choi, Y. Jung, S. B. Kim, H. J. Song, H. J. Shin, *Chem. Phys. Lett.* **2004**, *383*, 418–422.
- [44] E. Pulido Melián, O. González Díaz, J. M. Doña Rodríguez, G. Colón, J. A. Navío, M. Macías, J. Pérez Peña, *Appl. Catal. B* **2012**, *127*, 112–120.
- [45] P. Prieto, V. Nistor, K. Nouneh, M. Oyama, M. Abd-Lefdil, R. Díaz, *Appl. Surf. Sci.* **2012**, *258*, 8807–8813.
- [46] X. Liu, Z. Liu, J. Lu, X. Wu, B. Xu, W. Chu, *Appl. Surf. Sci.* **2014**, *288*, 513–517.
- [47] N. Maiti, S. Thomas, A. Debnath, S. Kapoor, *RSC Adv.* **2016**, *6*, 56406–56411.
- [48] H. W. Zhang, Y. F. Chen, L. Bao, Y. J. Yuan, *J. Catal.* **2022**, *412*, 1–9.
- [49] I. Lopez-Salido, D. C. Lim, Y. D. Kim, *Surf. Sci.* **2005**, *588*, 6–18.
- [50] A. J. Haes, R. P. Van Duyne, *Anal. Bioanal. Chem.* **2004**, *379*, 920–930.
- [51] A. L. C. M. Da Silva, M. G. Gutierrez, A. Thesing, R. M. Lattuada, J. Ferreira, *J. Braz. Chem. Soc.* **2014**, *25*, 928–934.
- [52] G. B. Strapasson, F. R. Scheffer, S. W. Cendron, F. d. C. Silva, N. H. Lazzari, C. Azambuja, A. Peyrot, D. E. Weibel, *SN Appl. Sci.* **2020**, *2*, 543.
- [53] A. M. D. Fornari, M. B. d. Araujo, C. B. Duarte, G. Machado, S. R. Teixeira, D. E. Weibel, *Int. J. Hydrogen Energy* **2016**, *41*, 11599–11607.
- [54] M. P. Languer, F. R. Scheffer, A. F. Feil, D. L. Baptista, P. Migowski, G. J. Machado, D. P. de Moraes, J. Dupont, S. r. R. Teixeira, D. E. Weibel, *Int. J. Hydrogen Energy* **2013**, *38*, 14440–14450.

---

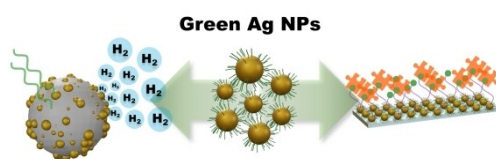
Manuscript received: January 2, 2023

Revised manuscript received: July 31, 2023

Accepted manuscript online: August 3, 2023

Version of record online: ■■, ■■

## RESEARCH ARTICLE



Silver NPs between 7.0 and 12.8 nm in size are prepared in diluted aqueous solutions containing only radish extracts or honey by microwave irradiation. The AgNPs are

assembled in a nanoplasmic biosensor chip for biomarkers detections and used as co-photocatalyst ( $\text{TiO}_2\text{@AgNPs}$ ) for hydrogen generation using UV or visible light.

*G. B. Strapasson, E. de C. Flach, Dr. M. Assis, Prof. S. A. Corrêa, Prof. E. Longo, Dr. G. Machado, Prof. J. F. L. Santos, Prof. D. E. Weibel\**

1 – 12

**Eco-friendly Synthesis of Silver Nanoparticles and its Application in Hydrogen Photogeneration and Nanoplasmic Biosensing**

